

Effects of Rate on Crack Growth in a Rubber-Modified Epoxy

J. Du¹, M. D. Thouless^{1,2} and A. F. Yee¹

¹ *Department of Materials Science and Engineering*

² *Department of Mechanical Engineering and Applied Mechanics
The University of Michigan, Ann Arbor, Michigan 48109, USA*

Abstract

The rate-dependent fracture behavior of a 10-phr rubber-modified epoxy was investigated using double-cantilever-beam tests at various crosshead speeds. Dramatic rate effects were observed in the R-curve behavior and in the relationship between the applied energy-release rate and the crack velocity. Furthermore, a transition between fracture with toughening mechanisms operating (kinetic crack growth) and brittle behavior (dynamic crack growth) was observed. This transition depended on the crack velocity and applied energy-release rate. Such behavior is expected to depend on how the intrinsic toughness and/or the extrinsic toughening mechanisms are influenced by strain rate. It was shown that the size of the process zone was only weakly dependent on the crack velocity until the onset of dynamic fracture. Furthermore, the extent of void growth was virtually independent of the crack velocity in the kinetic regime. These results appear to rule out the notion that crack-tip shielding is significantly affected by rate effects in this rubber-modified epoxy. Rather, the rate effects may arise from a rate-dependent intrinsic toughness. It was observed that the intrinsic toughness decreased significantly with increasing crack velocity. The crack instability was shown to be associated with an abrupt cessation of the development of the process zone, with both cavitation and void growth being totally suppressed.

Keywords: polymers, fracture and fracture toughness, embrittlement, crack velocity

March 2000

1. Introduction

The failure of a brittle material is governed not only by intrinsic properties, but also by external parameters such as the geometry, the loading configuration, and the rate of testing. These all interact to determine the mechanical response of the material. For example, the strength of a brittle material in the absence of kinetic effects is dictated by an instability that occurs when the crack-driving force, G , increases more rapidly with crack length than does the fracture resistance, R , [1, 2]. The rate of increase of G depends on the geometry of the specimen, while the rate of increase of R depends on the R-curve of the material. When crack growth is kinetic, the interdependence of the crack velocity, the applied energy-release rate, the extrinsic toughening mechanisms, and the intrinsic toughness of the material introduces additional complexities.

The relationship between crack-driving force and crack velocity has been studied for many polymers [3-11]. The crack velocity often appears to increase with crack-driving force until an instability occurs, after which it can increase with a decreasing applied energy-release rate. The stable portion of this behavior, where the crack-driving force increases with crack velocity, can be interpreted by cohesive-zone models [12-14] incorporating a rate-independent intrinsic toughness in which the visco-elastic dissipation around the crack tip scales with velocity. Several mechanisms have been proposed to describe the existence of unstable negative branches in curves of the energy-release rate *versus* crack velocity. Williams [3] assumed that local heating effects at the crack tip are responsible in PMMA. If the

local heating undergoes a transition from isothermal to adiabatic conditions when the crack velocity exceeds a critical value, material around the crack tip may soften at higher crack velocities, and, hence, exhibit a lower fracture resistance. Maugis [15] associated the toughness of visco-elastic materials with visco-elastic losses at the crack tip. In other words, the toughness was assumed to be dictated by the effect of strain rate on the constitutive properties of the material. The dissipated energy, and hence the toughness, is then related to the crack velocity because it is linked to the loss modulus of the material, which is frequency- (or strain rate-) dependent. Any decrease in the fracture resistance with increasing crack velocity is attributed to a significant reduction in the loss modulus at sufficiently high crack velocities so that the material tends to behave in a more elastic fashion.

An alternative model for unstable crack propagation involves a shielding mechanism at the crack tip [16]. In this model, the crack is assumed to be accompanied by a single craze which shields the crack tip [16]. The singular stress at the crack tip is characterized by a local stress-intensity factor, which is the difference between the applied stress-intensity factor and the shielding stress-intensity factor (associated with the tractions within the craze zone). The shielding stress-intensity factor was shown to be inversely dependent on the crack velocity and proportional to a power of the crack-tip stress-intensity factor. Then, by assuming a power-law relationship between the local stress-intensity factor and the crack velocity, it was shown that both stable and unstable behavior of the crack could be obtained. While the details of this model were developed for a crack propagating by a single craze, the

analysis incorporates all the mechanics that is expected to control steady-state crack growth in any polymer subject to crack-tip shielding.

Rubber-modified epoxies exhibit extrinsic toughening associated with shielding (or energy absorption) from the development of a process zone around the crack tip [17, 18]. Cavitation of the rubber particles and subsequent matrix deformation have been identified as the energy-absorbing mechanisms operating in this zone [17, 18]. Earlier work by the present authors investigated the phenomenon of R-curve development in these materials [19, 20]. It was demonstrated that the toughness increases with crack length as the process zone passes into the wake of the crack, exactly as would be expected with an extrinsic toughening mechanism. These tests were conducted under quasi-static conditions in which the crack was allowed to grow incrementally, and showed that the toughness increased from an initial value of about 1-2 kJm^{-2} to a steady-state value of between 5 and 8 kJm^{-2} , depending on the rubber content. Of particular note was the fact that the initial toughness appeared to be substantially greater than the toughness of the unmodified epoxy matrix (100-200 Jm^{-2}). The tests were all terminated by unstable crack growth when the process zone abruptly disappeared and the specimen failed catastrophically. While these tests provided considerable insight into the nature of the extrinsic toughening, practical applications of polymers often involve their use under conditions that can not be considered to be quasi-static. Experience shows that some polymers which appear to be quite promising under quasi-static tests may fail in a catastrophic fashion during service when rate effects are important. Therefore, the purpose of

the present work was to study the effects of rate on the development of R-curves, process zones, and crack-growth instabilities in a rubber-modified epoxy.

2. Experimental Results

The rubber-modified epoxy used in this work consisted of 100 parts (by weight) of a liquid diglycidyl ether of bisphenol-A epoxy (DER[®] 331 produced by the Dow Chemical Company), 10 parts of a liquid carboxyl-terminated acrylonitrile-butadiene copolymer rubber (HYCAR[®] CTBN 1300X8 produced by the B. F. Goodrich Company), and 5 parts of a curing agent (piperidine produced by the Aldrich Company). The material was cured at 120 °C for 16 hours.

The fracture behavior of this 10-phr (parts per hundred of resin) rubber-modified epoxy was studied using double-cantilever-beam tests. The geometry of the specimens is shown in Fig. 1. The samples were 6.35 mm wide, 40 mm thick and 110 mm long. Side grooves of depth 1.27 mm were used to keep the crack in the mid-plane of the specimens. An initial sharp crack about 40 mm long was formed by tapping a razor blade into the tip of a pre-machined notch. Tests were performed using a screw-driven Instron machine with crosshead speeds between 0.5 mm/min and 100 mm/min. A video-recording system was used to observe the propagation of the trace of the crack on the surface of the specimen. Features on the fractured surface were subsequently used to deduce approximate correlations between the location of the surface trace of the crack and the length of the crack in the middle of the specimen. The applied energy-release rate, G , for a crack of length a was determined using the equation [21]

$$G = \frac{12P^2(a + 0.668h)^2}{b_n E b h^3}, \quad (1)$$

where P is the applied load, h is the sample half-thickness, b is the sample width, b_n is the crack width (Fig. 1), and E is Young's modulus (2.6 GPa) [19]. Some examples of data relating the applied energy-release rate, G , and crack extension are shown in Fig. 2. The cracks began to propagate when G was between about 1.3 and 2.7 kJ/m². Eventually, the crack suddenly became unstable, and the specimen failed catastrophically. While there was a general tendency for the maximum value of G to depend on the crosshead speed, there was no unique relationship between the two parameters.

Video-images were also used to calculate the crack velocity. By correlating the crack velocity to the crack length and applied load, it was possible to establish relationships between the applied crack-driving force and crack velocity. The cracks remained stationary (but with a process zone developing ahead of the crack tip) as the applied energy-release rate was increased from zero to a critical value when they suddenly began to grow at a finite velocity. The transition to dynamic crack propagation (and complete failure) occurred within one video frame of 1/30 second. It was very clear that the crack did not accelerate in a continuous fashion to dynamic velocities. At very high loading rates, catastrophic failure occurred after the formation of a process zone with no intermediate stage of kinetic crack growth. Some examples (the same sets of data used to plot Fig. 2) of the relationship between the applied crack-driving force and crack velocity are shown in Fig. 3.

Thin sections perpendicular to the crack surface at the mid-plane of the fractured specimens were obtained by a combination of cutting, grinding and polishing until a final thickness of about 100 μm was reached [22]. The thinned sections were examined using transmitted light. Examples of the resulting micrographs, taken of the specimens used to generate the data of Figs. 2 and 3, are shown in Fig. 4. The process zone appears dark owing to the increase in light scattering caused by cavitation of the rubber particles and plastic deformation of the surrounding matrix. The characteristics of the evolution of the process zones are made clearer in the plots of Fig. 5 which show how the thickness varies along the length of the process zone. The boundary of the process zone was not distinct and the consequent uncertainty in identifying it is reflected in the error bars of this figure.

3. Discussion

Models of the type discussed in the Introduction generally predict a unique relationship between the applied energy-release rate and the crack velocity. However, it is clear from Fig. 3 that this is not the case for the material studied here. It is assumed that this results from a complex interaction between rate effects and the evolution of the process zone as the crack passes through the material. For a full understanding of this interaction, several individual phenomena need to be considered simultaneously. These include (i) how the applied energy-release rate depends on the crack length, crack velocity and loading rate; (ii) how the evolution of the process zone is influenced by the crack velocity and the applied energy-release rate; (iii) how the crack velocity is affected by the energy-release rate at the crack tip;

(iv) how the energy-release rate at the crack tip depends on the applied energy-release rate and on the extrinsic toughening provided by the process zone. Finally, the physics associated with the onset of the instability has to be understood. A complete modeling of these interactions is beyond the scope of this paper. However, further insight into the overall nature of the problem can be obtained by a closer examination of the experimental data associated with some of the separate phenomena.

3.1 Applied energy-release rate

It is important to appreciate that the variation of the applied energy-release rate, G , with crack length, a , should not be invested with too much significance. This can be seen by re-expressing Eqn. (1) in terms of the crosshead displacement, Δ , so that the relationship between G and a for a double-cantilever beam is of the form

$$G = \alpha \frac{\dot{\Delta}^2}{a^4} \quad (2)$$

where α depends on the specimen dimensions and the Young's modulus of the material. (For simplicity, the correction factor included in Eqn. (1) to account for the effects of shear is neglected here.) The rate of change of the applied energy-release rate, \dot{G} , is given by

$$\frac{\dot{G}}{G} = 2\frac{\dot{\Delta}}{\Delta} - 4\frac{\dot{a}}{a} \quad (3)$$

where $\dot{\Delta}$ is the crosshead speed, and \dot{a} is the crack velocity. If the crosshead speed is kept constant, as in these experiments, the applied energy-release rate will increase

when $\dot{a} < a/2t$, where t is the time elapsed after the beginning of the test. Conversely, G will decrease when $\dot{a} > a/2t$. The curves of applied energy-release rate against crack length will be very sensitive to parameters such as the precise loading conditions, geometry and how the crack velocity evolves with time. Therefore, the details of these curves may not be of much significance, and should not be considered as R-curves, unless, perhaps, they are obtained under quasi-static conditions (as in Ref. 19).

3.2 Evolution of the process zone

Micrographs such as those shown in Fig. 4 were used to determine the width of the process zone as a function of distance from the initial crack tip. If it is assumed that the width of the process zone at any location is actually a measure of the width when the crack tip reached that location, then, by correlating the crack extension to the applied energy-release rate and the crack velocity, it is possible to determine the width of the process zone as a function of both the applied energy-release rate and the crack velocity. The results of many measurements are shown in Fig. 6, in which the half-width of the process zone, h , is plotted against G for different crack velocities. This figure shows two significant results. The first is that the width of the process zone is only weakly dependent on the crack velocity. There may possibly be some rate effects at the high crack velocities, but, overall, rate effects do not appear to be significant in determining the size of the process zone. The second result is that the half-width of the process zone is proportional to the applied

energy-release rate. There is a linear dependence on G , where the half-width in μm is given by

$$h = 30-50G \quad (4)$$

(and G is in kJ/m^2). This linear dependence is consistent with models of the evolution of a process zone [23-26]¹. These models indicate that the half-width of a dilatational process zone under plane-strain conditions is expected to be given by

$$h = 2 \times 10^5 \frac{G}{\sigma_c^2}, \quad (5)$$

where h is in μm , σ_c is the critical stress required to trigger non-linear deformation in the process zone (in MPa), and G is in kJ/m^2 . (Young's modulus has been taken to be 2.6 GPa [19] while Poisson's ratio has been taken to be 0.4.) A comparison between Eqns. 4 and 5 suggests a critical stress is in the range of 60-80 MPa which is consistent with the results of uniaxial tests on this material.

The strain, and hence the extent of plastic deformation around the cavitating particles is expected to vary through the process zone. To examine this, fractured specimens were cleaved perpendicular to both the fracture surface and the direction of crack growth. The resulting sections were coated with a thin sputtered film of gold and examined using secondary-electron imaging in a scanning-electron microscope. An example of a composite micrograph is shown in Fig. 7. The process zone of this specimen had a nominal half-width of $150 \pm 30 \mu\text{m}$ according to

¹ In Ref. [19], an incorrect statement about how the process zone size varies with applied energy-release rate was made by mistake.

measurements made using transmission-optical techniques. Figure 7 shows that the percentage of cavitated rubber particles varied from approximately 100% at the crack surface, to about 60% at 150 μm from the crack surface, and was approximately 0% at a distance of 2 mm from the crack surface. The volume-fractions of the non-matrix portions of these sections were calculated from this micrograph using image-analysis techniques. The results are shown in Fig. 8 as a plot of the volume fraction of non-matrix phase against distance from the crack surface. It will be noted that the volume fraction was approximately 16% throughout most of the process zone. The volume fraction dropped to approximately 10% over a small transition region, and remained constant at this lower level out to locations well away from the process zone. This lower limit is in excellent agreement with the expected volume fraction of the rubber particles calculated from the composition and densities of the modified epoxy. These results suggest that after cavitation, the voids increase in volume by about 60% before fracture occurs. The sizes of the process zones reported in Figs. 5 and 6 appear to correspond to the region in which void growth occurs; the upper-bound corresponds to the region over which the voids reach their maximum size, and the lower-bound corresponds to the point at which the matrix begins to exhibit appreciable plastic deformation.

The fracture surfaces of the samples were also examined and analyzed by scanning-electron microscopy. Figure 9 illustrates the contrasting appearance of the fracture surfaces between the regions of dynamic failure and crack growth at lower velocities. Figure 10 indicates the volume fractions of the non-matrix phase at different crack speeds. These results indicate the extent of void growth

corresponding to the point at which cohesive fracture occurs in the matrix. It can be seen that there appears to be no effect of crack velocity on this quantity in the kinetic regime. In all cases, the volume fraction of voids was close to 16.6% on the fracture surface. This is comparable to the results of Fig. 8, and indicates that the stress is approximately hydrostatic within the process zone. After the instability, there was neither cavitation nor void growth; at just over 10%, the volume fraction of the non-matrix portion corresponded to the expected volume-fraction of the rubber particles. It should be noted that if there was any transient void expansion that relaxed immediately after fracture it would not be detected in these observations.

3.3 Effects of velocity on intrinsic toughness

The discussion of the previous section appears to rule out the notion that crack-tip shielding is significantly affected by rate effects in this material. However, the experimental results indicate very clear rate effects on the behavior, even well away from the region of instability. This could arise from a connection between the velocity and the crack-tip energy-release rate, which would be equivalent to the notion of a rate-dependent intrinsic toughness for the modified epoxy.

It was observed that while the crack remained stationary, a process zone began to develop ahead of it as the applied energy-release rate was increased. Then, at a critical value of G , the crack suddenly began to grow with a characteristic velocity. The formation of a process zone ahead of a stationary crack does not provide any extrinsic toughening. Therefore, the critical values of G (the initial points on the curves of Fig. 2) correspond to the intrinsic toughness of the material. Figure 11

shows how the intrinsic toughness for the modified epoxy decreases with increasing crack velocity. Crack growth data for the pure epoxy is superimposed on this figure so as to provide a comparison between the behavior of the rubber-modified epoxy and the matrix material. The large difference between the intrinsic toughness of the rubber-modified material and the toughness of the pure epoxy suggests that different mechanisms must contribute to the decohesion processes at the crack tip. In an unmodified epoxy, chain scission (with some deformation) is expected to be important. In the modified epoxies, rubber cavitation, matrix void growth and subsequent chain scission along the crack plane are all expected to contribute to the decohesion process.

Two points need to be specifically addressed in reference to Fig. 11: the significance of the intrinsic toughness and the significance of the initial velocity. The first point to emphasize is that there is no process zone behind the original crack tip; therefore it is the intrinsic toughness being measured in these experiments.² Evidence of this was provided in Ref. [18] where micrographs of the process zone obtained using transmission optical microscopy (TOM) show it starting from the original crack tip. Further evidence was provided by additional TOM studies in which the original starter crack was examined before testing. These studies confirmed that there was no process zone in the wake of the original crack, but a small process zone of half-width 10 μm existed ahead of the crack. This is

² This is consistent with observations that the initial crack tip went straight across the sample despite the fact that, owing to plane-stress effects, the process zone ahead of the crack was much larger on the free surfaces than in the middle of the specimen. After some crack growth had occurred, the crack trailed at the free surface because of the increased toughening caused by the process zone after it had passed into the wake of the crack.

consistent with the notion that a razor blade tapped into the material introduces a crack that initially grows at dynamic velocities with no process zone before being arrested. The geometry of the initial crack indicated that it was arrested when the applied energy-release rate dropped to about 100 or 200 Jm^{-2} (approximately the toughness of the pure epoxy). After the crack was arrested, it was subjected to an energy-release rate of this level while the razor blade remained in place, and a process zone had time to form ahead of the now stationary crack. The relationship between the size of this process zone and the applied energy-release rate is entirely consistent with the rest of the data shown in Fig. 6. During the fracture experiments, this initial process zone was subsumed into the process zone that developed before crack growth. No difference is expected between the features of the process zone in the experiments described here, and those that would be observed upon loading a perfectly “sharp” initial crack (which would also develop a process zone ahead of the crack before fracture). In both cases, the intrinsic toughness can be obtained because extrinsic toughening essentially occurs only when the process zone passes into the wake of the crack.

The experiments indicated very clearly that when the cracks began to grow, they did so at a well-defined velocity. No gradual acceleration from zero velocity was observed, and the apparent absence of any region where the crack velocity increased with intrinsic toughness was noteworthy. The almost-two-orders-of-magnitude change in the initial velocity shown in Figure 11 seems to rule out the notion that this observation might be associated with some limitations of detection. Furthermore, this figure provides a clear correlation between the crack velocity and

crack-tip energy-release rate that had been clearly missing in the earlier attempt to relate the crack velocity to applied energy-release rate (Fig. 3).

3.4 Transition to the instability

All the experiments were terminated by an instability in which the crack propagation suddenly changed from a kinetic regime (associated with cavitation in the process zone) to a dynamic regime (with no cavitation in the process zone). This transition was essentially instantaneous. In less than one video frame (1/30 second) from the point of instability, the crack advanced across the entire specimen causing catastrophic failure. While at low and intermediate loading rates, the instability occurred after some crack extension, at high loading rates the crack extended dynamically after developing a small process zone at the tip without any kinetic crack propagation. Nonlinear deformations (*e.g.* rubber cavitation and matrix void growth) were totally suppressed after the instability, and the crack propagation may have approximately followed the curve for pure epoxy shown in Fig. 11. Generally, the cracks were so over-driven at the instability point that they reached the end of the specimens before being arrested. However, the notion that the crack was arrested when the energy-release rate fell approximately to the level of the toughness of the epoxy matrix was confirmed in another study using a similar system [27], and was also indicated by the observations made on the initial crack introduced by a razor blade.

Models of instability such as those discussed in the introduction generally suggest that there should be a critical crack velocity or a critical crack-tip energy-

release rate at which the instability occurs. This was investigated by determining the crack velocity just before the onset of instability. However, Fig. 12 shows that instead of there being a single value of the critical velocity, there was a range in which the critical velocity was inversely dependent on the applied energy-release rate. Figure 11 indicates that this corresponds to a range of crack-tip energy-release rates of about 1.5 kJm^{-2} and lower. At relatively high deformation rates, dynamic fracture occurred after the development of an initial process zone with no intermediate stage of kinetic crack growth. Both the applied energy-release rate at which failure occurred, and the extent of the process zone that formed ahead of the original crack tip before catastrophic failure, decreased with increasing deformation rate. For example, at a loading rate that corresponded to $\dot{G} = 1 \text{ kJm}^{-2}\text{s}^{-1}$ catastrophic failure occurred when $G = G_{\text{tip}} = 1.1 \text{ kJm}^{-2}$.

4. Conclusions

Nonlinear deformations (e.g. rubber cavitation, void growth and matrix shear deformation) are responsible for the formation of a crack-tip process zone in rubber-modified epoxies. R-curve behavior associated with the extrinsic toughening induced by this process zone has been confirmed in prior studies [19, 20]. The present study demonstrates a linear correlation between the size of the process zone and the applied crack-driving force (Fig. 6). This is consistent with process-zone toughening models [23-26] and supports the notion that linear fracture mechanics is a suitable framework for analyzing the fracture of these materials. However, practical applications for toughened brittle polymers require an understanding of

the rate-dependent fracture behavior. Strong rate effects on crack propagation are demonstrated in Figs. 2 and 3. Two regimes of crack growth were observed: a kinetic and a dynamic regime. Kinetic crack growth was slow enough to be monitored optically, and was accompanied by the development of a process zone ahead of the crack. At relatively low crack velocities, a transition occurred where the process zone suddenly stopped forming, and the crack velocity jumped to a dynamic range.

Models of rate-dependent crack growth in polymers often incorporate a crack-tip shielding that has a strong dependence on the crack velocity [12-14, 16]. However, Fig. 6 shows that for the rubber-modified epoxy studied here, the size of the process zone is only weakly dependent on the crack velocity in the kinetic regime. Furthermore, as shown in Fig. 10, there is no obvious reduction in the extent of cavitation and void growth as the crack accelerates within the kinetic regime. While the effects of rate on extrinsic toughening appear to be limited in the kinetic regime, the results of Fig. 3 clearly show a significant (but not unique) relationship between the applied energy-release rate and crack velocity, culminating in a sudden and dramatic embrittlement. This is believed to arise from the dependence of the intrinsic toughness of the material on crack velocity. A crack grows by decohesion processes such as chain disentanglement and scission occurring at the crack tip. The tractions and displacements associated with these processes give rise to the intrinsic toughness of the material, which can be measured from the initial portion of an R-curve. The experimental results presented here, and in Refs. 19 and 20, suggest that the intrinsic toughness of a rubber-modified epoxy can be an order of magnitude larger than that of an unmodified epoxy. Figure 11

demonstrates that these decohesion processes are very sensitive to rate, and that there is an inverse relationship between the intrinsic toughness and crack velocity. This effect seems to be sufficiently large that changes in the intrinsic toughness, rather than in the extrinsic toughening, may be the most important contribution to rate sensitivity in these materials.

The critical crack velocity at which the toughened-to-brittle transition occurs is inversely dependent on the applied energy-release rate (Fig. 12). This transition is associated with an abrupt end to the cavitation process (Figs. 4 and 5), and an instantaneous elevation of the crack velocity to the dynamic range. Once cavitation has ceased, the fracture properties of the modified epoxy appear to mimic approximately those of the unmodified epoxy. Currently, it is not clear whether the transition in fracture modes occurs because of the rate-dependence of the intrinsic toughness, or because of a competition between the onset of voiding and cleavage at the boundary of the process zone. While rubber-modified epoxies are capable of excellent levels of extrinsic toughening, their practical use depends on avoiding fracture instabilities that limit impact resistance. Understanding the toughened-to-brittle transition may be very important, as similar effects may occur in other brittle polymers toughened by extrinsic mechanisms.

Acknowledgments

This work is supported by the National Science Foundation under Grant CMS-9523078. The authors are thankful to P. C. Niven and R. G. Hutchinson for experimental help.

References

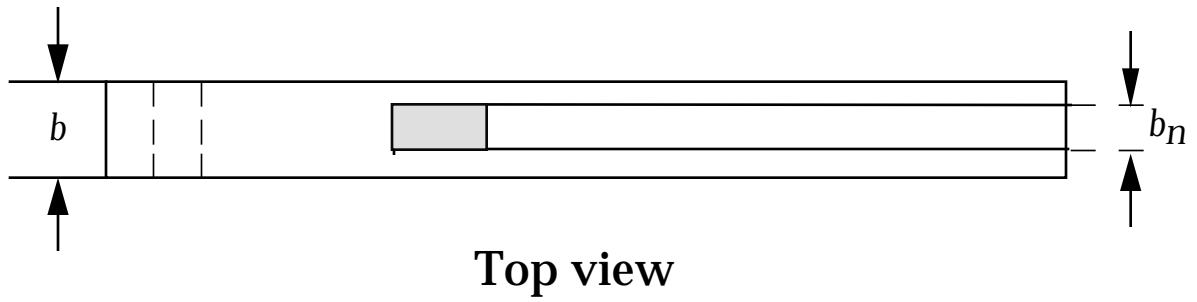
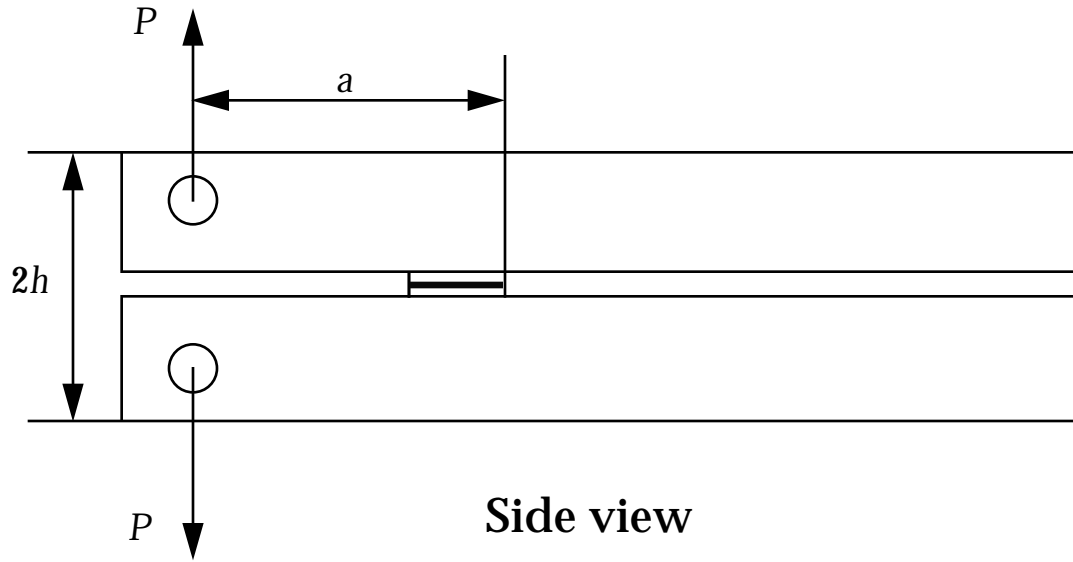
1. Mai, Y.-W. and Lawn, B. R., *Ann. Rev. Mater. Sci.*, **1986**, **16**, 415.
2. Cook, R. F. and Clarke, D. R., *Acta Metall.*, **1988**, **36**, 555.
3. Williams, J. G., *Int. J. of Fract.*, **1972**, **8**, 393.
4. Atkins, A. G., Lee, C. S. and Caddell, R. M., *J. Mater. Sci.*, **1975**, **10**, 1381.
5. Marshall, G. P., Culver, L. E. and Williams, J. G., *Int. J. Fract.*, **1973**, **9**, 295.
6. Parvin, M. and Williams, J. G., *J. Mater. Sci.*, **1975**, **10**, 1883.
7. Andrews, E. H. and Stevenson, A., *J. Mater. Sci.*, **1978**, **13**, 1680.
8. Chan, M. K. V. and Williams, J. G., *Polymer*, **1983**, **24**, 234.
9. Hine, P. J., Duckett, R. A. and Ward, I. M., *J. Mater. Sci.*, **1984**, **19**, 3796.
10. McGarry, F. J., Mandell, J. F. and Lee, L. H., *J. Polym. Sci. Polym. Symp.*, **1985**, **72**, 83.
11. Takemori, M. T., Morelli, T. A. and McGuire, J., *J. Mater. Sci.*, **1989**, **24**, 2221.
12. Williams, M. L., in *Fracture of Solids* (Eds: Drucker, D. C. and Gilman, J. J.), Interscience Publishers, New York, NY (1963) pp. 157.
13. Knauss, W. G., in *Deformation and Fracture of High Polymers* (Eds: Kausch, H. H. and Jaffee, R.), Plenum Press, New York, NY (1973) pp. 501.
14. Schapery, R. A., *Int. J. Fract.*, **1975**, **11**, 141.
15. Maugis, D., *J. Mater. Sci.*, **1985**, **20**, 3041.
16. Kramer, E. J. and Hart, E. W., *Polymer*, **1984**, **25**, 1667.

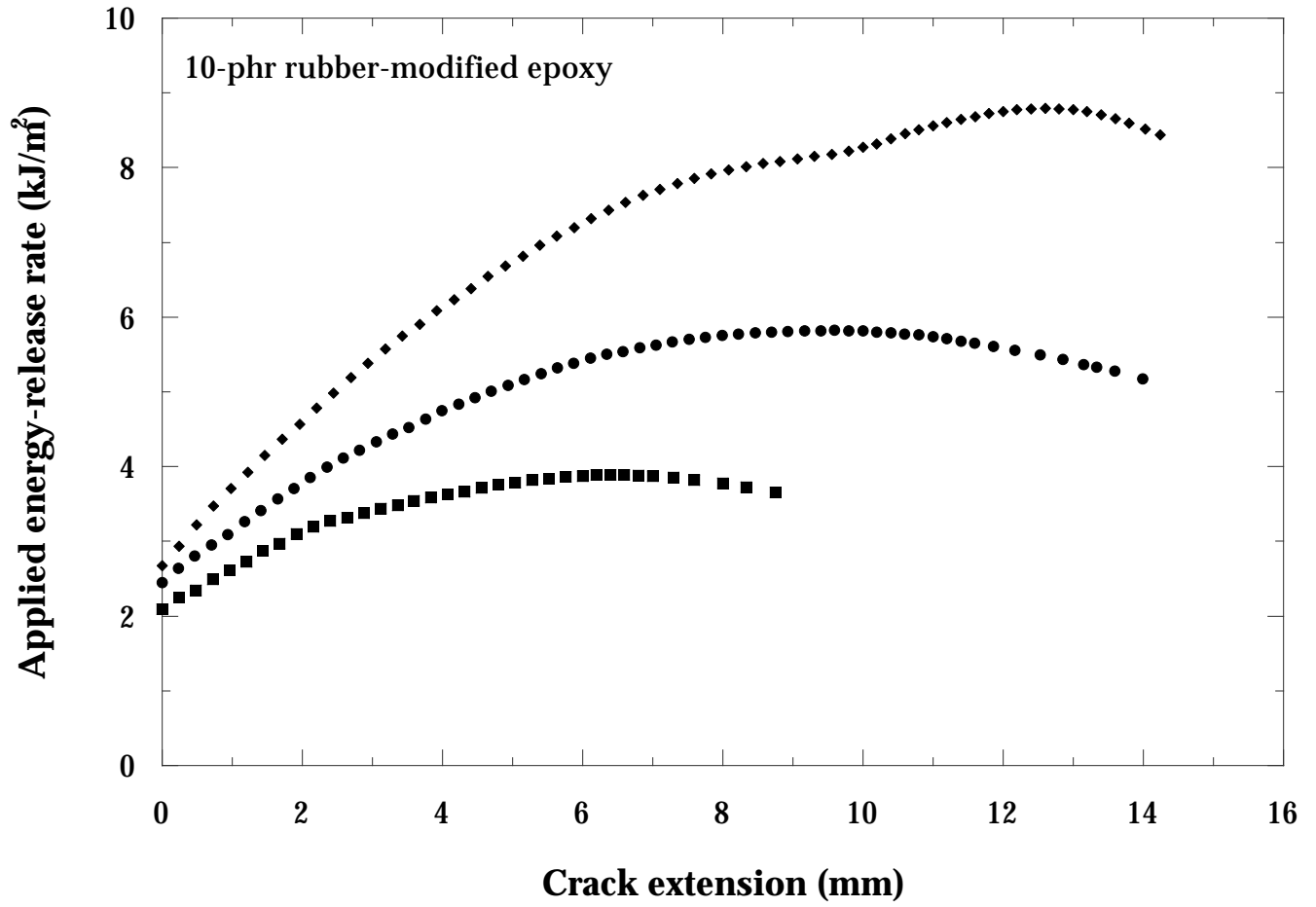
17. Kinloch, A. J., Shaw, S. J., Tod, D. A. and Hunston, D. L., *Polymer*, **1983**, **24**, 1341.
18. Pearson, R. A. and Yee, A. F., *J. Mater. Sci.*, **1986**, **21**, 2475.
19. Du, J., Thouless, M. D. and Yee, A. F., *Int. J. Fract.*, **1998**, **92**, 271.
20. Thouless, M. D., Du, J. and Yee, A. F., in *Toughening of Plastics* (Eds: Pearson, R. A., Yee, A. F. and Sue, H. J.), in press.
21. Wiederhorn, S. M., Shorband, A. M. and Moses, R. L., *J. Appl. Phys.*, **1968**, **39**, 1569.
22. Holik, A. S., Kambour, R. P., Hobbs, S. Y. and Fink, D. G., *Microstruct. Sci.*, **1979**, **7**, 357.
23. McMeeking, R. M. and Evans, A. G., *J. Am. Ceram. Soc.*, **1982**, **65**, 242.
24. Budiansky, B., Hutchinson, J. W. and Lambropoulos, J. C., *Int. J. Solids Struct.*, **1983**, **19**, 337.
25. Evans, A. G., and Faber, K. T., *J. Am. Ceram. Soc.*, **1984**, **67**, 255.
26. Tvergaard, V. and Hutchinson, J. W., *J. Mech. Phys. Solids.*, **1992**, **40**, 1377.
27. Du, J., Ph.D. Thesis (University of Michigan, Ann Arbor, MI), **2000**.

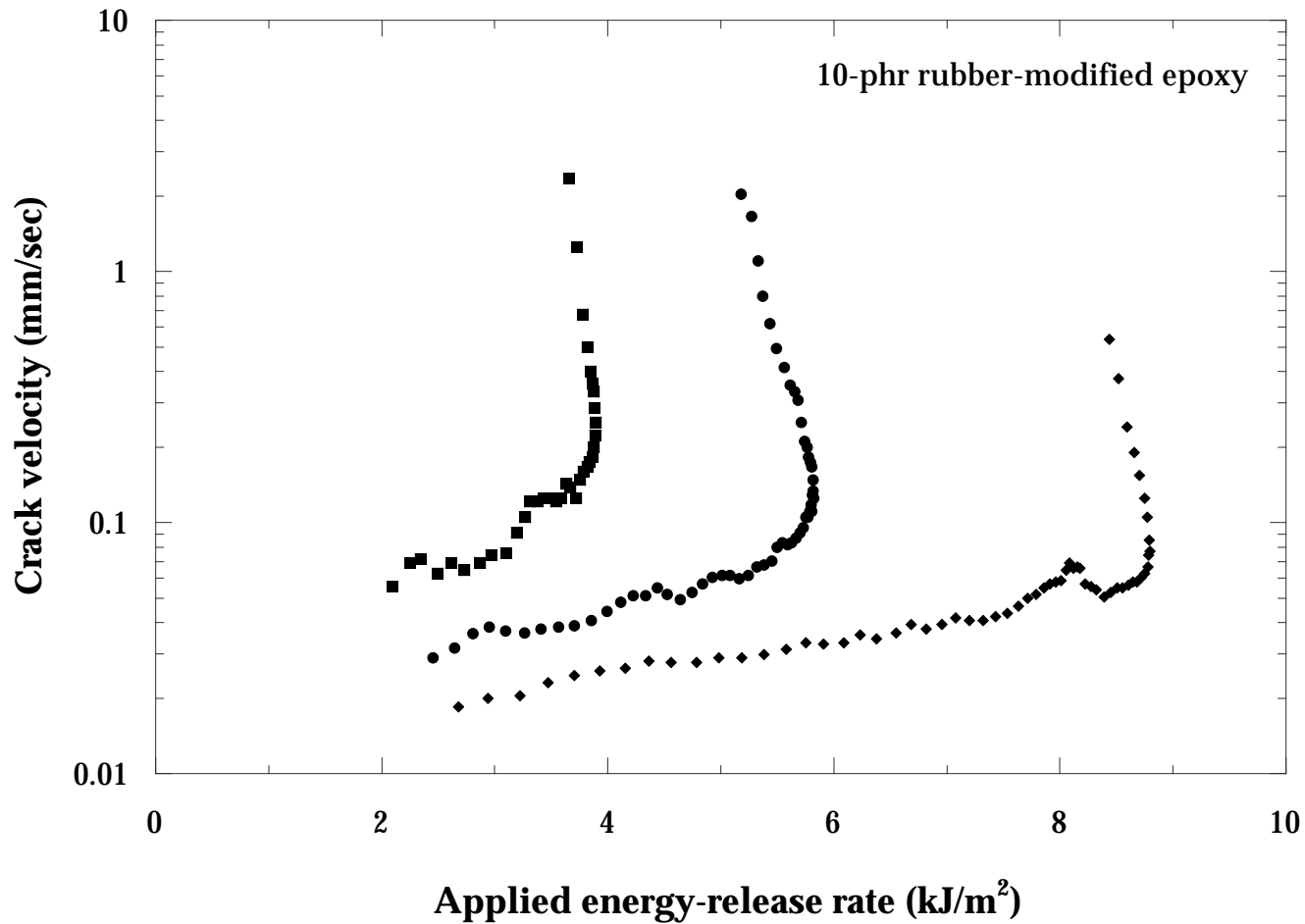
Figure captions

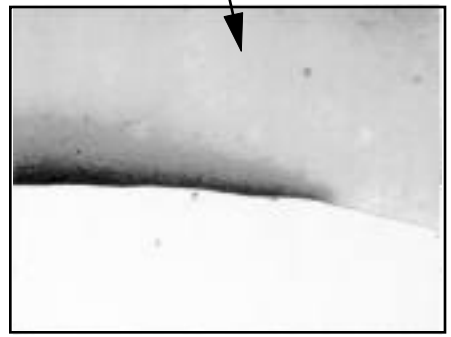
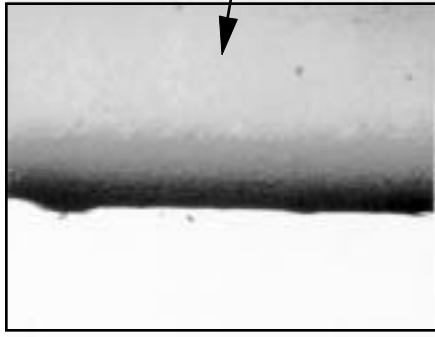
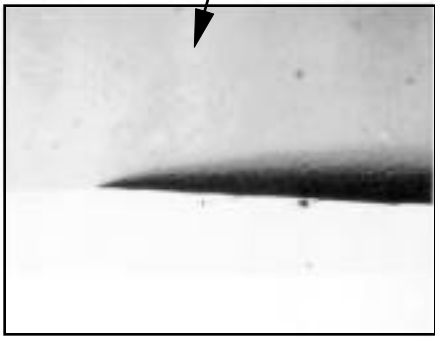
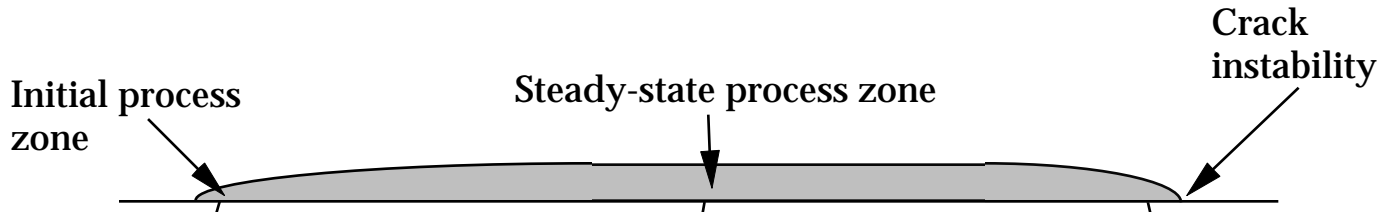
- Figure 1** Diagram of the double-cantilever-beam specimens used in this work. The sample width, b , was 6.35 mm, and the sample thickness, $2h$, was 40 mm. Side grooves of depth 1.27 mm were used to keep the crack in the mid-plane of the samples.
- Figure 2** Examples of plots for the applied energy-release rate against crack extension for a 10-phr rubber-modified epoxy. The data for the three curves shown were obtained from experiments in which the crosshead speeds were 1 mm/min (◆), 1.5 mm/min (●), and 2 mm/min (■).
- Figure 3** Characteristic plots of crack velocity *versus* the applied energy-release rate curves for the 10-phr rubber-modified epoxy. The curves are associated with the data of Fig. 2, and correspond to crosshead speeds of 1 mm/min (◆), 1.5 mm/min (●), and 2 mm/min (■).
- Figure 4** Transmission optical micrographs of the process zones for the 10-phr rubber-modified epoxy. These micrographs show the three samples used to obtain the data presented in Figs. 2 and 3, and correspond to crosshead speeds of 1 mm/min, 1.5 mm/min, and 2 mm/min.
- Figure 5** Thickness (half width) of the process zone plotted against distance along the process zone for the 10-phr rubber-modified epoxy. The data were obtained from the three micrographs shown in Fig. 4, and correspond to crosshead speeds of 1 mm/min (◆), 1.5 mm/min (●), and 2 mm/min (■).
- Figure 6** Thickness (half-width) of process zone plotted against applied energy-release rate at 3 crack velocities (◇ -- 0.05 mm/sec, ○ -- 0.2 mm/sec, □ -- 1 mm/sec) for the 10-phr rubber-modified epoxy. (The data were obtained from 14 samples tested with 7 crosshead speeds between 0.5 mm/min and 2.5 mm/min.)

- Figure 7** Scanning electron micrographs of a section through the process zone taken perpendicular to the fracture surface. The nominal half-width of the process zone was 150 μm . The micrograph was taken from a specimen tested at 2 mm/min, and a point where $G = 3.7 \text{ kJ/m}^2$ and the crack velocity was 0.4 mm/sec.
- Figure 8** Volume fraction of non-matrix portions as a function of distance from the crack surface, obtained from the micrograph of Fig. 7. The solid line represents the volume fraction of the rubber particles calculated from the compositions of the 10-phr rubber-modified epoxy and the density of each component.
- Figure 9** Scanning electron micrographs of (a) slow-crack-growth and (b) fast-crack-growth fracture surfaces for the 10-phr rubber-modified epoxy tested with a crosshead speed of 2 mm/min.
- Figure 10** Volume fractions of the non-matrix portion of fracture surfaces from the kinetic regime, plotted against crack velocity for the 10-phr rubber-modified epoxy tested with a crosshead speed of 2 mm/min. The solid line represents the volume fraction of the rubber particles calculated from the compositions of the 10-phr rubber-modified epoxy and the density of each component.
- Figure 11** Crack velocity plotted as a function of intrinsic toughness for the 10-phr rubber-modified epoxy (\bullet). Superimposed on this plot are data obtained for the pure epoxy matrix (\circ).
- Figure 12** Critical crack velocity just before the transition between kinetic and dynamic fracture, plotted as a function of applied energy-release for the 10-phr rubber-modified epoxy.

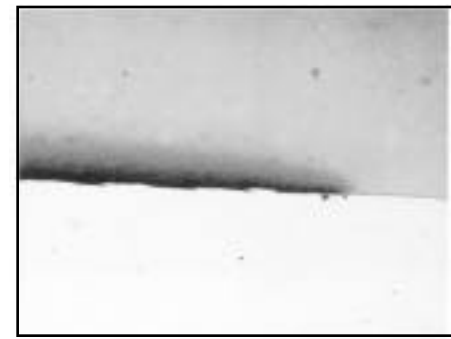
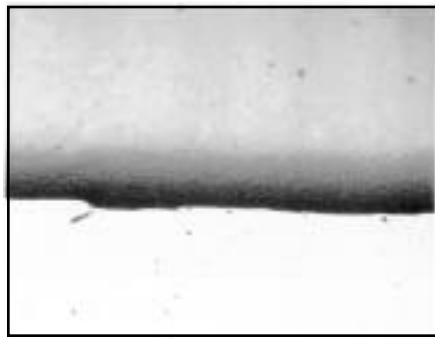




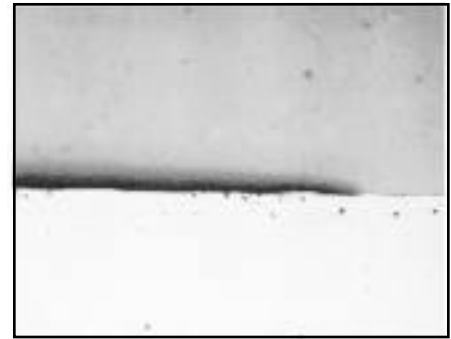
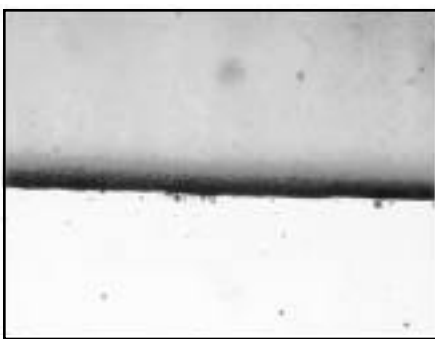




1 mm/min

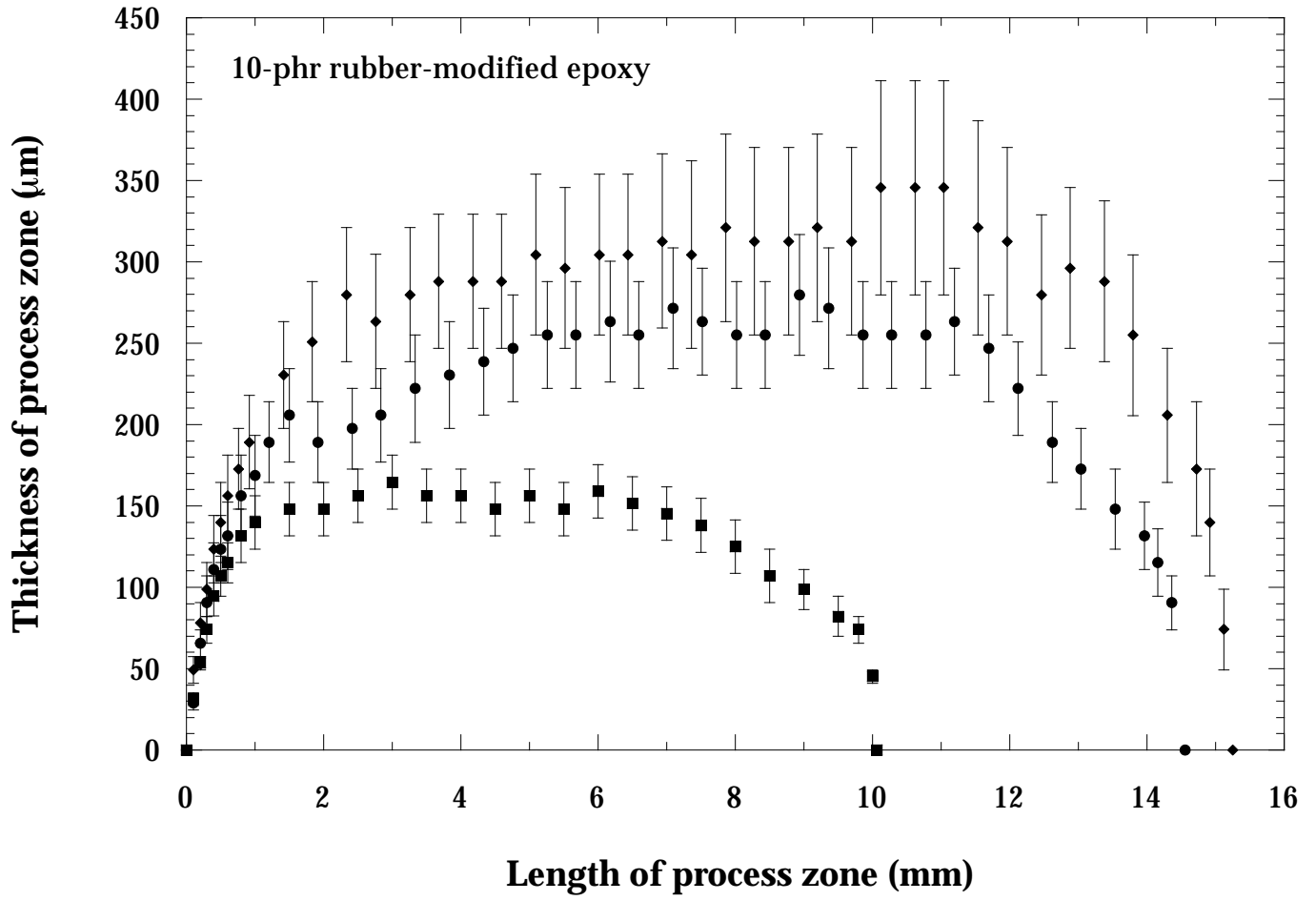


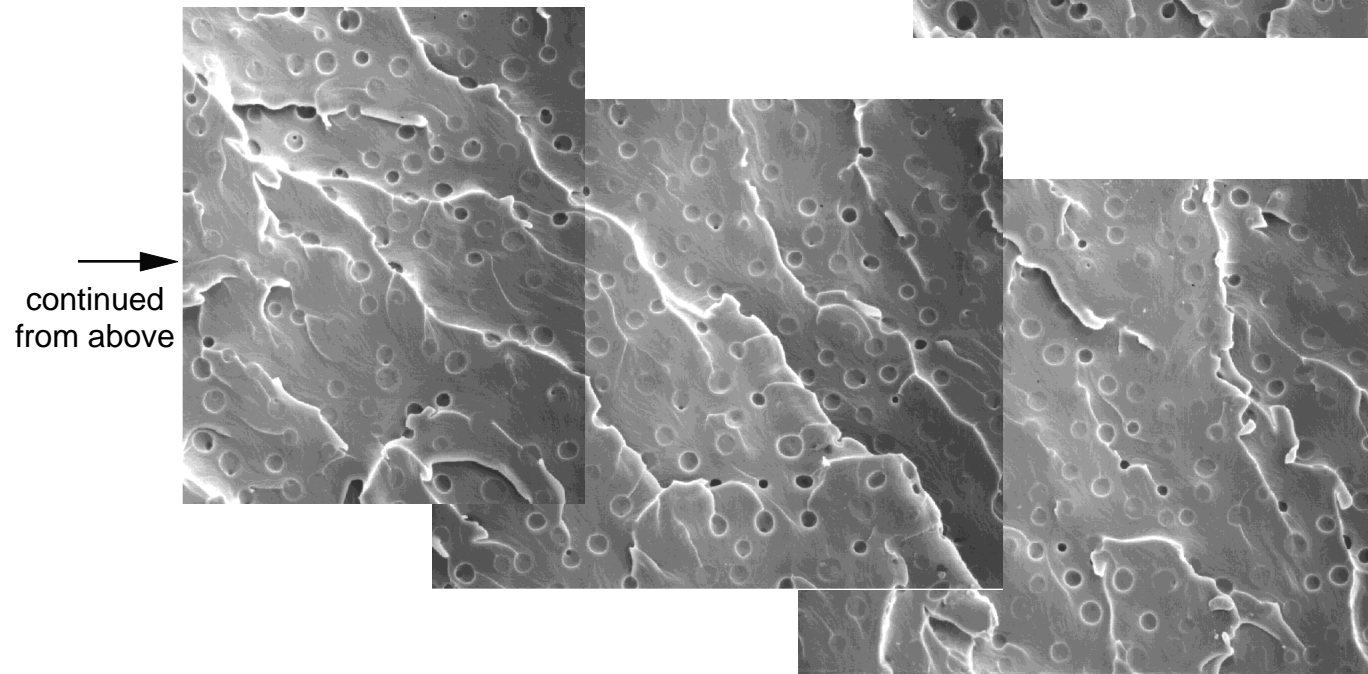
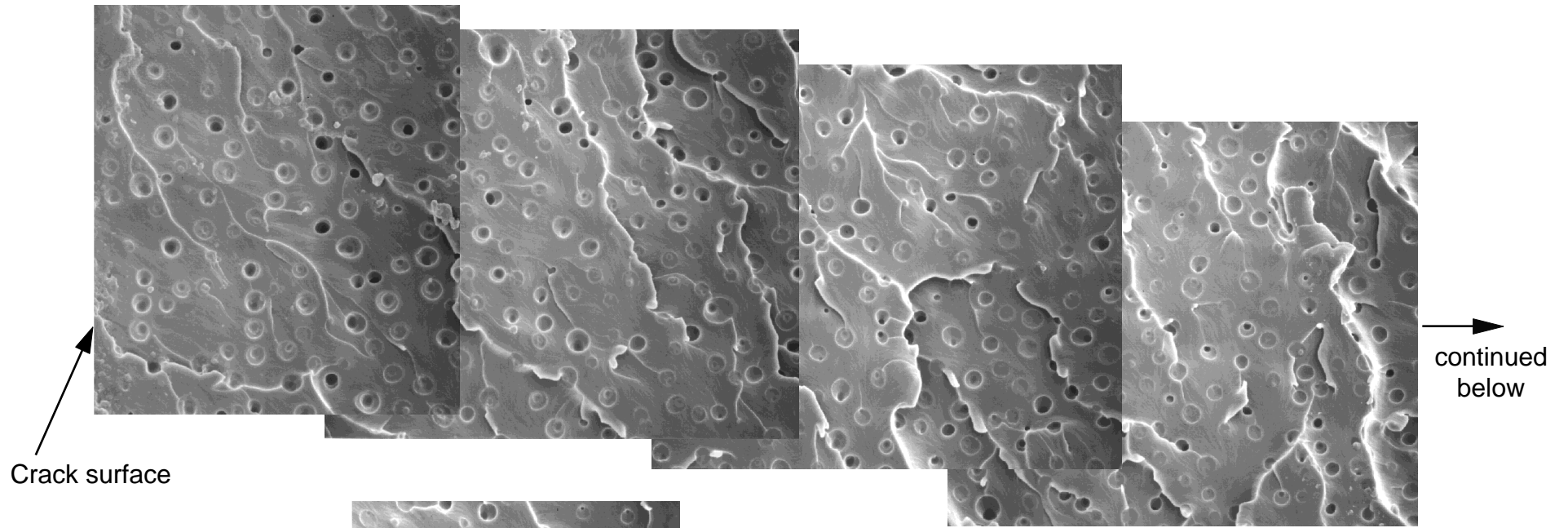
1.5 mm/min




2 mm/min

400 μm

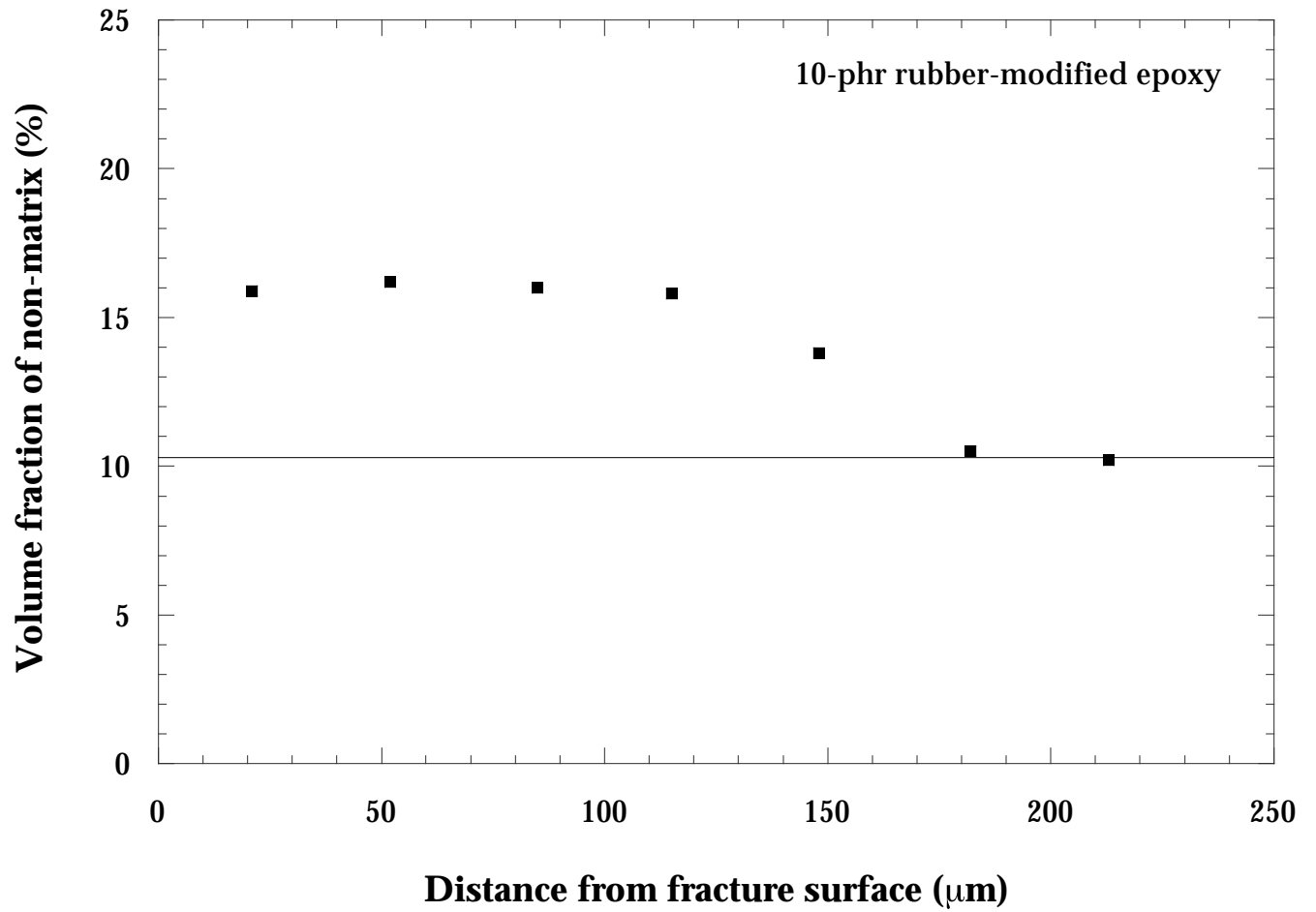


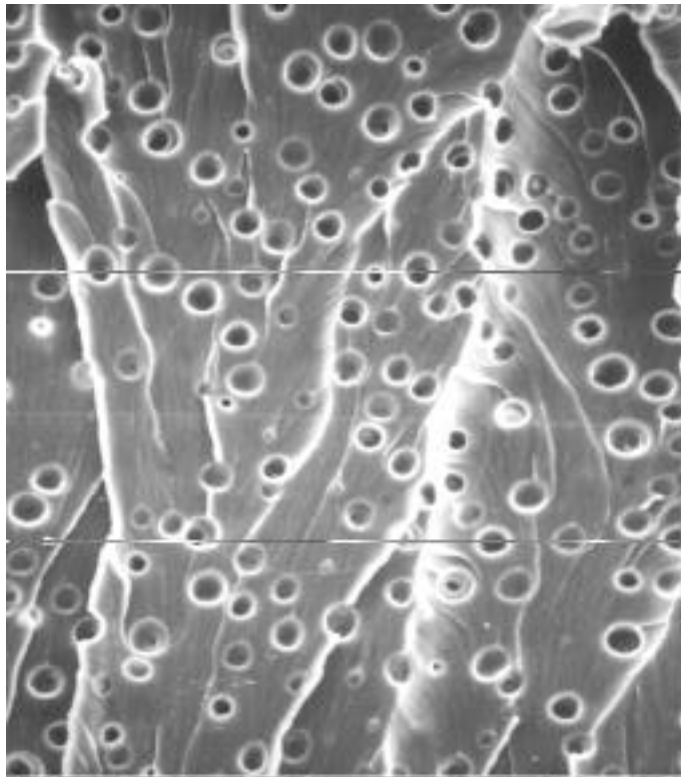


15 μm



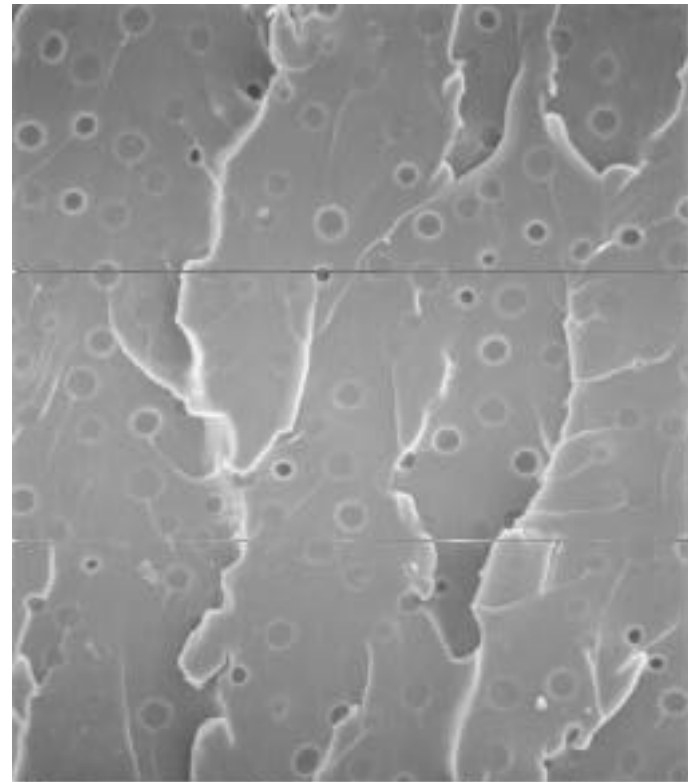
A horizontal scale bar is located below the text "15 μm ".





3 μm

(a)



3 μm

(b)

